MDPI

Article

Application of Seismic Waveform Indicator Inversion in the Depth Domain: A Case Study of Pre-Salt Thin Carbonate Reservoir Prediction

Jinjin Hao [1,*], Shiguo Wu [2], Jinxiu Yang [3], Yajun Zhang [1] and Xuemei Sha [1]

[1] Research Institute of Petroleum Exploration and Development-Northwest, PetroChina, Lanzhou 730020, China
[2] Institute of Deep-Sea Science and Engineering, Chinese Academy of Sciences, Sanya 572000, China
[3] School of Geosciences, China University of Petroleum (East China), Qingdao 266580, China
[*] Correspondence: haojinjin@petrochina.com.cn

Abstract: Prestack depth-migrated seismic data, having more accurate imaging position and amplitude fidelity than prestack time-migrated seismic data, are supposed to produce a higher quality reservoir prediction result by using depth-domain inversion. Some researchers have developed different methods of depth-domain seismic inversion. However, it has not been widely used in the industry probably because of two reasons: (1) it is a complex process to conduct depth-domain seismic inversion due to the nonstationary depth-domain seismic wavelet; and (2) time-domain seismic inversion is considered capable of solving the problem with less cost, both in regard to time and the economy. In this paper, we try to use the seismic waveform indicator inversion method in the depth domain. First, a forward model was built to demonstrate that seismic waveforms both in the time domain and the depth domain are highly correlated with lithologic associations. Second, a quantitative evaluation method of seismic data for reservoir prediction was proposed, which can help geophysicists estimate time-domain and depth-domain inversion effects before inversion. Finally, the seismic waveform indicator inversion method was implemented for presalt thin carbonate reservoir prediction in the Central Block at the eastern margin of the Pre-Caspian Basin. The depth-domain inversion result shows a relatively true structure and higher resolution validated by wells.

Keywords: depth-domain seismic inversion; seismic waveform; Pre-Caspian basin

1. Introduction

Seismic inversion refers to the process of converting seismic boundary reflections into layer properties [1]. It plays a vital role in reservoir characterization for hydrocarbon exploration and development. The reliability and accuracy of inversion results highly rely on the seismic imaging quality. In the last three decades, rapid strides in seismic imaging technology have been made in developing depth migration algorithms and procedures. Prestack depth migration, such as Kirchhoff, one-way wave, and reverse time migration, has gradually become the mainstream imaging technology. Given an accurate velocity-depth model, prestack depth migration overcomes velocity pull-up and push-down effects, enables the calculation of more accurate volumetric parameters, and also improves vertical and lateral resolution by properly aligning events [2]. Prestack depth migration has a more accurate imaging position and a higher imaging fidelity amplitude than prestack time migration, especially in geologically complex environments that are usually favorable for oil and gas accumulation, such as subsalt, foreland thrust belts, fault blocks, reefs, etc. However, the dominant application of prestack-migrated seismic data remains structure interpretation. Depth-domain seismic inversion has not been extensively used in the industry probably because of two reasons: (1) it is a complex process to conduct depth-domain seismic inversion due to the nonstationary depth-domain seismic wavelet; and

(2) time-domain seismic inversion is considered capable of solving the problem with less cost, both in regard to time and the economy.

To invert depth-migrated seismic data directly, there are basically two directions. One is the deterministic method based on the convolution model, and the other is geostatistical inversions based on stochastic simulation.

The convolution model assumes that the seismic wavelet is time-invariant and has a single phase. Each seismic trace is a convolution result of the subsurface reflectivity and the wavelet [3]. Depth-domain and time-domain seismic wave fields are interrelated, and their mathematical expressions are similar [4]. It has been proven that the basic concepts of wavelet and convolution are also applicable to the depth domain [5]. However, the depth-domain wavelet has the characteristic of spatial variation. It varies while traveling through layers of different velocities and elongates as velocity increases. It cannot be estimated from seismic data by statistical methods directly as the time-domain wavelet [6]. The strong nonstationarity of the depth-domain wavelet makes it difficult to implement seismic inversion directly in the depth domain [7,8]. Chen et al. [9,10] used the phase independence of the envelope for attempts to solve the problem of wavelet spatial variation, which might provide a reference to depth-domain seismic wavelet extraction. Singh [11] developed a deterministic depth-domain inversion workflow for petrophysical properties with calibrated well-log data. Fletcher et al. [12] proposed a formulation of the seismic inversion and imaging in the depth domain by using point-spread functions as a kernel matrix. The method was later applied to process seismic data sets from the Gulf of Mexico and western China [13]. Zhang et al. [14] presented a depth-domain inversion method by using the compressed sensing technique with an output of reflectivity and band-limited impedance. Zhang and Deng (2018) proposed a new wavelet extraction method by using the depth-wavenumber decomposition technique, which can generate depth variant wavelets to accommodate the nonstationarity of the depth-domain seismic data [15]. Despite all the attempts, the complex calculation process of deterministic inversion methods caused by the nonstationary depth-domain seismic wavelet still restricts their application in the industry.

Geostatistical inversion can establish relationships between well-log data and depth-domain seismic data based on statistical principles and directly estimate lithology and reservoir without depth-domain wavelet extraction [16]. It has been applied in fault block reservoirs, tight-gas fields, and other complex geological settings [17,18]. However, traditional geostatistical inversions use limited samples to characterize the spatial variability and estimate the high-frequency components of prediction points. The simulation results are affected by the distribution of the sample points, therefore, requiring a relatively uniform distribution. In addition, the statistics of the variogram cannot accurately reflect the change in sedimentary facies in reservoir space. It leads to poor planar geological regularity and strong randomness in simulation results [19]. To address the issue of seismic waveform indicator inversion, a novel high-precision inversion method based on traditional geostatistical inversion has been developed. It uses the lateral change in seismic waveform instead of the variogram to characterize the spatial variability of reservoirs under the constraints of the stratum framework [20].

In this paper, we try to use the seismic waveform indicator inversion method in the depth domain. Firstly, we demonstrated that depth-domain seismic waveforms are highly correlated with lithologic associations through a forward model. Thus, we can apply the seismic waveform indicator inversion method to invert prestack depth-migrated seismic data directly without depth-domain seismic wavelet extraction. Secondly, we established a method for quantitatively evaluating the time-domain and depth-domain seismic data before inversion, which can help geophysicists estimate inversion effects in advance and reduce calculation costs. Finally, the seismic waveform indicator inversion was carried out for presalt thin carbonate reservoir prediction in the Central Block at the eastern margin of the Pre-Caspian Basin. The depth-domain inversion result shows a relatively true structure and a higher resolution than the time-domain inversion, which are validated by wells. The

evaluation and inversion methods are recommended for use in other areas with complex geological environments.

2. Method

2.1. Forward Model

Seismic waveforms contain a variety of seismic kinematics and dynamic information, which are a comprehensive response to sedimentation, lithology, reservoir physical properties, fluid, and other geological information. Similar sedimentary characteristics often have similar lithologic associations, and similar lithologic associations often result in similar seismic waveform characteristics. If the seismic waveforms around wells are similar in the target layer, it indicates that the wells are in roughly the same sedimentary environment. Although the high-frequency components of the P-wave impedance may come from different sedimentary microfacies, the middle and low frequencies have common characteristics, and the common frequency band range greatly exceeds the effective seismic frequency band [21].

First of all, a forward model was built to demonstrate the relationship between lithologic associations and seismic waveforms. Figure 1 shows a carbonate geological model and its corresponding prestack time migrated seismic reflection result (Figure 1b) and prestack depth migrated seismic reflection result (Figure 1c). A 30-Hz Ricker wavelet is applied in the model. The carbonate reservoir's (green rectangles) thickness is 4 m, which is far below the seismic resolution. The velocity is 4000 m/s, and the density is 2.88 g/cm^3. The background mudstone (yellow) has a velocity of 3000 m/s and a density of 2.29 g/cm^3. As shown in Figure 1b,c, without the influence of complex structure, noise, and other factors, the seismic waveforms of prestack time migrated data and prestack depth migrated data are very similar, showing a consistent conclusion that seismic waveforms are highly correlated with lithologic associations. Well X has the same lithologic association as Well A, and therefore shares a similar seismic waveform as Well A; Well B has a different lithologic association with Well X, and therefore produces a different seismic waveform from Well X, even though Well B is closer to Well X. It builds on the foundation of using the seismic waveform indicator inversion method to invert prestack depth migrated data directly without depth-domain wavelet extraction.
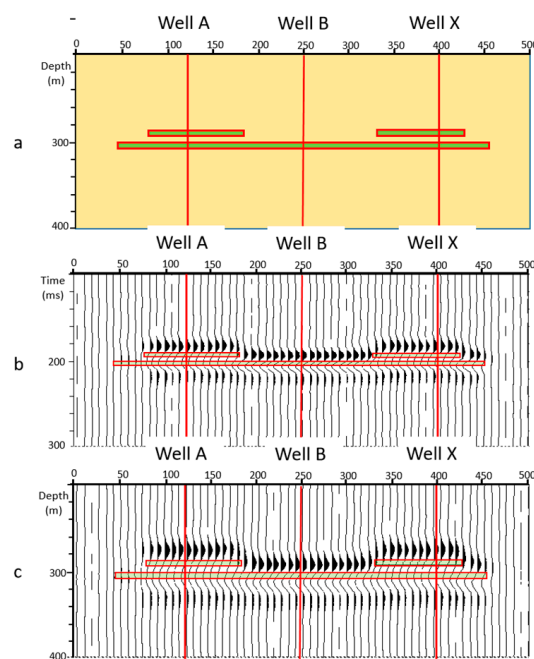

Figure 1. Geological model (**a**) and its corresponding seismic reflections: prestack time migrated data (**b**) and prestack depth migrated data (**c**).

2.2. Evaluation of Depth-Domain Seismic Data

The improvement of seismic data on structural imaging is easy to observe, while the improvement of reservoir prediction ability is difficult to evaluate. Although previous studies have exhibited that prestack depth-migrated seismic data has higher accuracy and resolution than prestack time migrated seismic data, its improvement for seismic inversion is rarely quantitatively evaluated before inversion. Based on the relationship between seismic waveforms and logging curves, we established a method to quantitatively evaluate time-domain and depth-domain seismic data. As shown in Figure 2, the target interval of the two wells has similar seismic waveforms both in the time domain and depth domain. The correlation coefficients (R) are 81% and 79%, respectively. In the time-domain inversion, logging curves are usually resampled to 2 or 1 ms to match the time-domain seismic data. Information beyond 0–200 Hz is lost during the process of well-to-seismic calibration. The logging curves are basically the same when applying 0–600 Hz, 0–500 Hz, 0–400 Hz, and 0–300 Hz filtering. The correlation coefficient of the original P-impedance curve of the two wells is only 66% because of the high-frequency component. After filtering out the high-frequency components, the common structure of the two logging curves is left, which can be used to build the initial model. When we filter the P-impedance curve gradually from 0–600 Hz to 0–100 Hz, the correlation coefficients of the P-impedance curves are gradually increased to 88% in the time domain and 90% in the depth domain. When the correlation coefficient of the two logging curves is as high as the correlation coefficient of seismic waveforms, the frequency bandwidths of the logging curves are 0–200 Hz in the time domain and 0–300 Hz in the depth domain. It means that the depth-domain inversion can retain 0–300 Hz of well log data in the initial model, which is higher than the time-domain inversion, and consequently produce a higher resolution result.
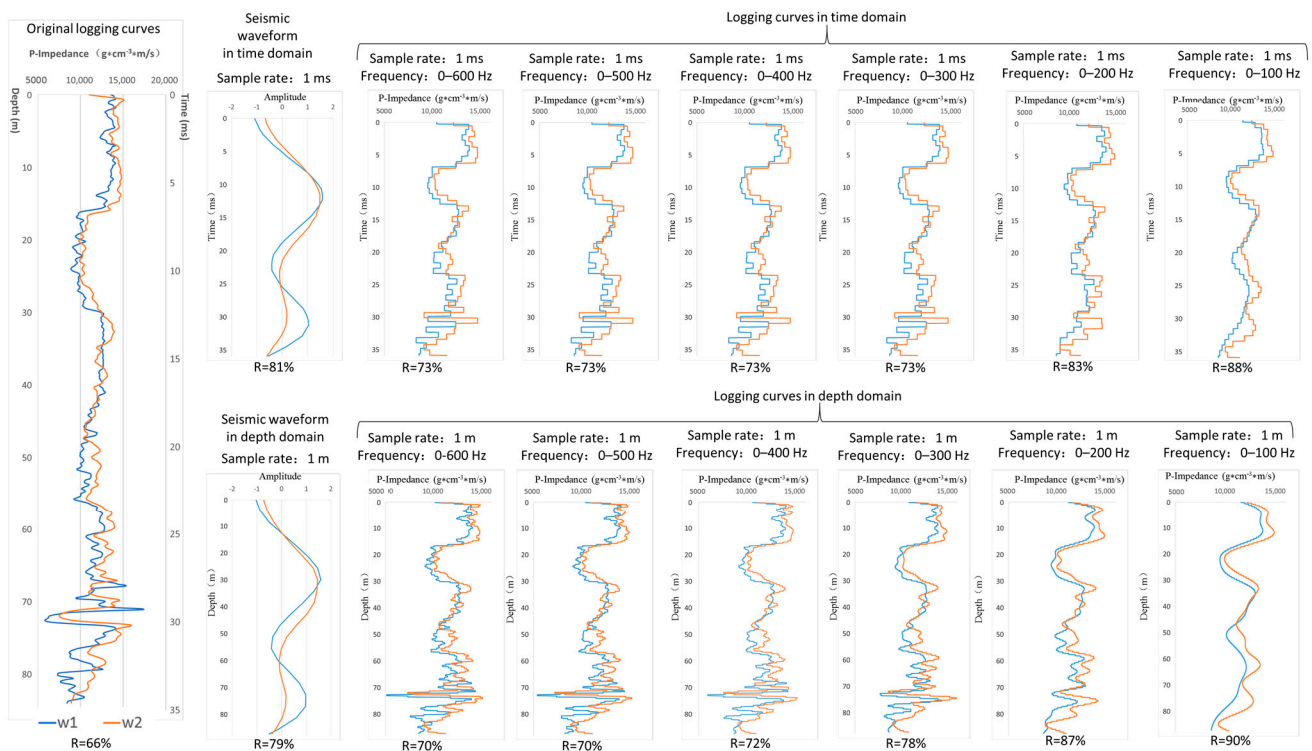

Figure 2. Logging curve comparison of two wells (w1 and w2) with similar seismic waveform at different frequency bandwidths.

2.3. Seismic Waveform Indicator Inversion

The workflow of seismic waveform indicator inversion is shown in Figure 3. It mainly includes 4 steps:
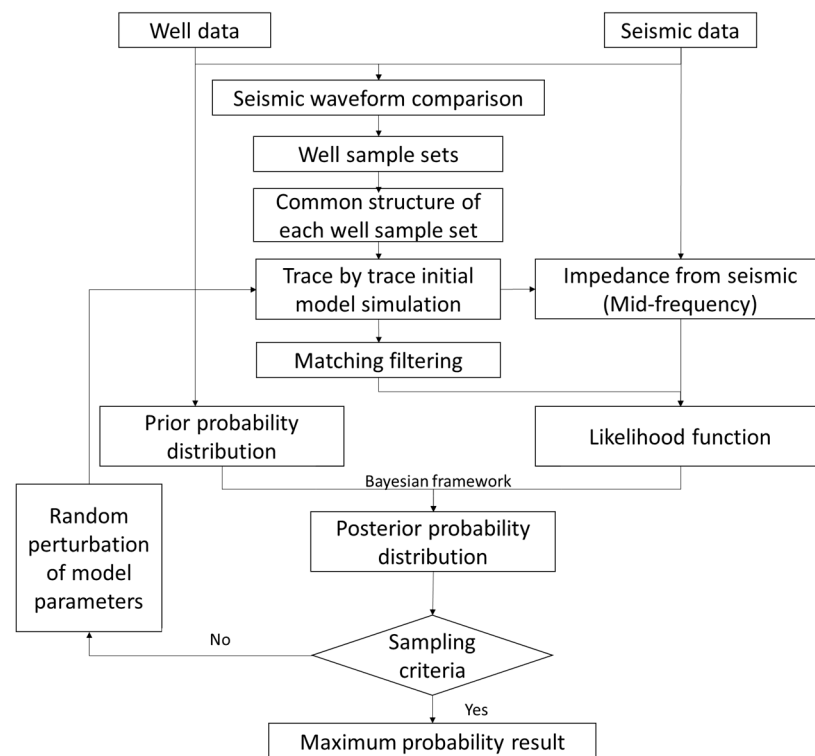
Figure 3. The workflow of seismic waveform indicator inversion.

Firstly, the initial sample set of different seismic waveform structures is generated based on singular value decomposition. The corresponding relationship between seismic waveform and well point attributes can be defined as a n × m order matrix A. Next, perform orthogonal decomposition on A. When the rank of the matrix is r, then matrix A can be decomposed into the algebraic sum of *r* eigenvectors, and the total energy of matrix A can be expressed as:

$$\|A\| = \sum_{i=1}^{r} \delta_i^2 \tag{1}$$

In which, δ_i is the non-negative square root of the AA^T eigenvalue.

After the orthogonal decomposition of matrix A in Equation (1), the main characteristics of matrix A can be represented by the singular vector corresponding to the first *r* nonzero singular values. Then, efficient dynamic clustering analysis of seismic waveform structures can be achieved, and the initial sample set of different seismic waveform structures can be established.

Secondly, the common structure of all logging curves in each sample set is extracted. The logging curves in each sample set are decomposed into low-medium frequency (macro feature), high frequency (detail), and ultra-high frequency (noise) by using Equation (2) to carry out discrete wavelet transforms with different cut-off frequencies. The extracted low-medium frequency is the common structure of all logging curves in the sample set.

$$O(f) = \arg\left(\min\|W - \overline{W}\|\right) = \arg\left(\min\left\|\int_0^l \varphi(\omega,t)d\omega - \overline{W}\right\|\right) \tag{2}$$

where *f* is the cut-off frequency related to the common structure, *W* is the logging curve of the sample well set, $\overline{W}$ is the average value of the logging curve of the sample well set, and $\varphi(\omega,t)$ is the wavelet function.

Thirdly, the initial model can be built trace by trace based on both seismic waveform similarity and spatial distance. The seismic waveform of the predicted point is compared with the seismic waveform of drilled wells. All wells are sorted, and wells with high seismic waveform similarity and a small space distance are selected to build the initial model.

Finally, constrained by the Bayesian framework, the initial model is constantly modified according to the actual seismic waveform, so that the inversion results conform to the intermediate frequency seismic information and well-curve structure characteristics at the same time, and obtain a high-resolution waveform indicator inversion result. According to the definition of Bayesian condition probability, the posterior probability of the model parameter *m* under the condition of observation data *n* can be expressed as:

$$P(m \mid n) = \frac{p(n \mid m)p(m)}{\int p(n \mid m)p(m)dm} \propto p(m)p(n \mid m) \tag{3}$$

In which, *m* is the model parameter, $p(m)$ is the prior probability of the model that was acquired from the well logging data. *n* is the observation data, and $p(n)$ is the probability of *n*. $p(n \mid m)$ is the likelihood function, that is, the conditional probability under the known model. The prior probability of the model can be obtained from:

$$P(m \mid I) = \frac{1}{\sqrt{2\pi \mid \sigma_m \mid}} exp^{\left[-\frac{m^T m}{2\sigma_m}\right]} \tag{4}$$

where *I* is the prior information, σ_m represents the variance of the model.

The likelihood function is computed by conducting a matching filtering between the initial model and seismic impedance. It can be expressed as:

$$P(d \mid m, I) = \frac{1}{\left(\sigma\sqrt{2\pi}\right)^N} \times exp\left[-\frac{\sum_{n=1}^{N}(\Delta d_n - G\cdot\Delta m_n)^2}{2\sigma^2}\right] \tag{5}$$

Substitute Equations (4) and (5) into Equation (3), we have:

$$
\begin{aligned}
P(m \mid n) &\propto p(m)p(n \mid m) = P(m \mid I) \times P(d \mid m, I) \\
&= \frac{1}{2\pi^{\frac{3}{2}}\sqrt{det|\sigma_{\Delta m}|^3}} exp^{\left[-\frac{m^T m}{2\sigma_m}\right]} \times \frac{1}{\left(\sigma\sqrt{2\pi}\right)^N} \times exp\left[-\frac{\sum_{n=1}^{N}(\Delta d_n - G\cdot\Delta m_n)^2}{2\sigma^2}\right]
\end{aligned} \tag{6}
$$

In which, Δm is the perturbation quantity of the model parameter, and $\sigma_{\Delta m}$ is the variance of Δm. For a given seismic waveform *d*, the expected value of model *m* can be obtained using Gibbs sampling. The maximum probability solution of Equation (6) is the result of the inversion. Take the logarithm of Equation (6), and the objective function is obtained:

$$O(m \mid d, I) = -\frac{1}{2\sigma^2}\sum_{n=1}^{N}(G\cdot\Delta m_n - G\cdot\Delta m_n)^2 - \frac{\Delta m^T \Delta m}{2\sigma_{\Delta m}} \tag{7}$$

In order to achieve maximum posterior probability, we took the derivative of Equation (6) with respect to the model parameter Δm, and obtained:

$$O'(\Delta m) = \frac{1}{\sigma^2}\left[G^T G\Delta m - G^T \Delta d\right] - \frac{\Delta m}{\sigma_{\Delta m}} \tag{8}$$

Let $O'(\Delta m)=0$, then the model disturbance quantity is:

$$\Delta m = \left[GG^T + \frac{\sigma^2}{\sigma_{\Delta m}}I\right]^{-1}G^T \Delta d \tag{9}$$

The final high resolution inversion result is obtained by approximating the sample data with the method of selecting the perturbations of the model.

3. Application

3.1. Geological Settings

Pre-Caspian Basin is one of the most important petroliferous basins in the Eastern European Craton [22]. It has more than 200 oil and gas fields [23]. The Central Block is located at the eastern margin of the Pre-Caspian Basin, just west of the Ural fold belt, with a total area of 3280 km². Structurally, it belonged to the carbonate platform slope where the eastern Astrakhan-Aktyubinsk uplift extends to a southeast depression (Figure 4). The eastern Astrakhan-Aktyubinsk uplift has transformed gradually from a terrigenous clastic shelf to a carbonate platform shelf margin since the early carboniferous, with over 1000 m thickness of carbonate sequences. The carbonate strata are associated with large concentrations of hydrocarbons [24].
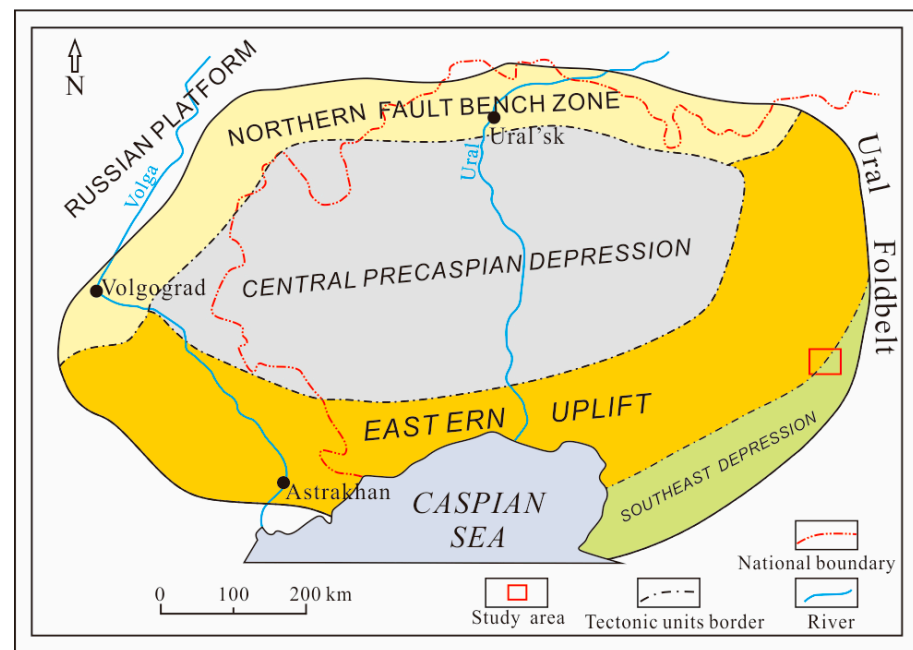
Figure 4. Tectonic settings and location of Central Block.

Due to strong compression of overlying sediments, giant salt domes have been formed in the Permian Kungurian formation. It played a critical role in preserving oil and gas in the Central Block [25]. The thickness of salt beds varied greatly, from tens of meters to kilometers. Underlying the salt domes, the carboniferous KT-I and KT-II thick carbonates, separated by a unit of terrigenous strata (MKT) are the primary target layers in the study area (Figure 5).

Carboniferous carbonate sequences in the Central Block have experienced two stages of sea-level rise and fall cycles. The upper carbonate formation was deposited during cycle 2 from the upper Moscovian to the Gzhelian, which is referred to as KT-I. The lower carbonate formation was developed during cycle 1 from the upper Visean to the lower Moscovian, which is referred to as KT-II (Figure 6). KT-II is further divided into Г, Д, and ТР-III, in which Г is the major oil layer. KT-II is dominated by open platform sediments, including four sedimentary microfacies: bioclastic beaches, debris beaches, beach depressions, and mudflats. The lithology of KT-II is mainly pure, brittle, low-shale content limestone, including: light gray micritic limestone, micritic bioclastic limestone, a small amount of bright bioclastic limestone, and argillaceous limestone.
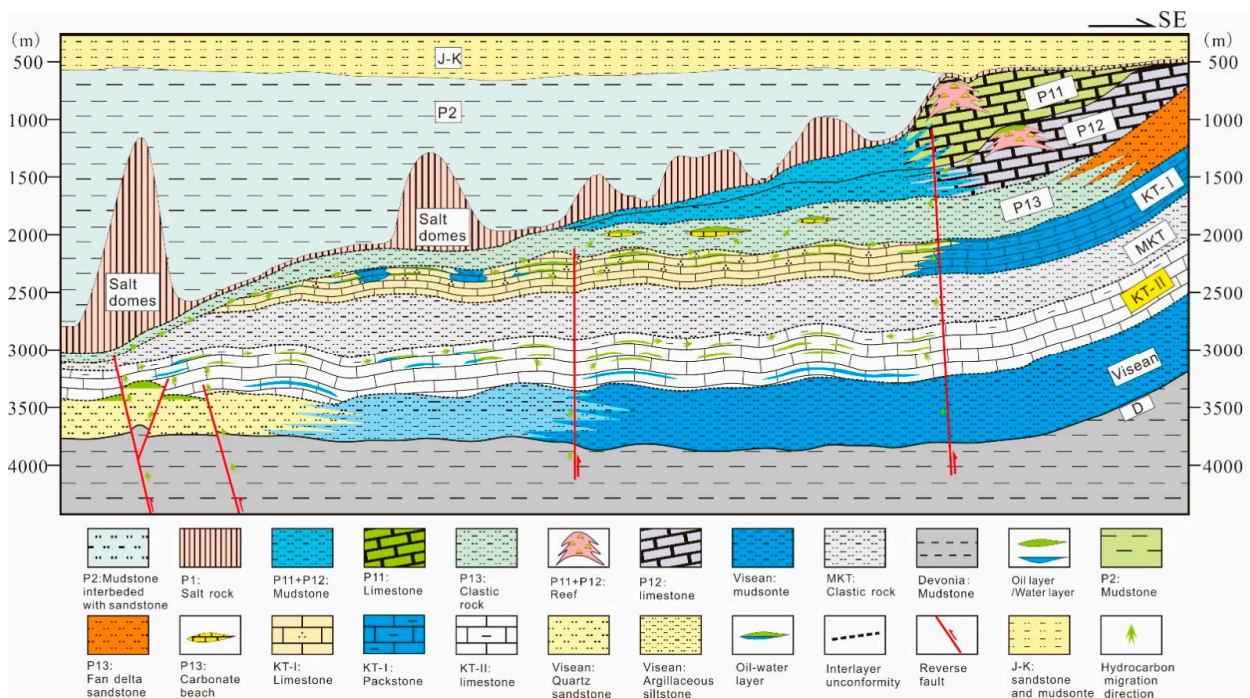
Figure 5. Hydrocarbon accumulation model of Central Block.

Figure 6. Regional stratigraphy in the study area.

The prevalent sedimentary microfacies in the early stage and diagenesis in the later stage jointly determine the development of the reservoirs in KT-II. A geological study suggests that bioclastic limestone in the Central Block, subjected to later dissolution due to the influence of periodic sea level fluctuation, has enlarged pore spaces and forms high-quality reservoirs. The main reservoir space is intragranular and intergranular dissolved pores. These reservoirs are thin layers superimposed vertically and are highly heterogeneous laterally. Well data statistics suggest that single reservoir thickness is mostly 1–4 m. Seismic data show parallel/sub-parallel, continuous reflections without distinct architecture. Conventional seismic methods have great difficulties in identifying carbonate reservoirs in KT-II.

3.2. Depth Migrated Seismic Data

The study area is fully covered by 3D seismic data. Frequency analysis suggests that the main frequency of the prestack time-migrated seismic data at the target layer is approximately 30 Hz, with the bandwidth ranging from 6 to 70 Hz. The narrow frequency bandwidth of seismic data causes difficulties in amplitude preservation and resolution enhancement. In addition, the thickness of Permian salt domes in the eastern margin of the Pre-Caspian Basin produces drastic lateral variations in velocity and leads to seismic events that cause distortion of presalt layers and poor imaging quality.

High-resolution 3D seismic data are the foundation of reservoir prediction, which directly determines the accuracy of the prediction result. It is necessary to acquire depth-domain seismic data in view of the problems existing with time-domain seismic data. In this paper, depth-domain seismic data was acquired with the techniques of well-constrained velocity modeling and reverse-time depth migration based on fine interpretation of salt domes and presalt structures. The imaging technique of reverse-time depth migration is a quite accurate migration method developed in the field of geophysical exploration in recent years. It adopts the two-way wave equation migration to deal with the imaging problems in geologically complex areas. The result possesses high imaging precision, and is not affected by the lateral velocity variation or steep structures [26].

The depth-domain imaging can better illustrate the boundaries of salt domes (black arrows) and presalt structure (yellow arrows) compared with seismic data in the time domain (Figure 7). The depth migration technique eliminated pull-up effects (yellow arrows) on seismic time profiles, which are caused by overlying salt domes with high velocity in the Central Block. The presalt structures can have more accurate reflection repositioning. Additionally, on the depth-domain seismic section, the wave group characteristics are clearer, and the continuity of wave group events in the carboniferous KT-I and KT-II formations is obviously enhanced (blue ellipse), which is favorable for horizon tracking and fine structural interpretation.

Besides better imaging quality for structure interpretation, it is very important to evaluate the data for reservoir prediction. The main frequency of the depth-domain seismic data is approximately 35 Hz, with a bandwidth from 5 to 80 Hz. More well-log data were selected to implement the previous evaluation process. The final statistical results are shown in Table 1. The first line of the table comes from Figure 2. By comparing the data in column 2 and column 4, we can find out that the depth-domain seismic data can retain a higher frequency band range of well log data than time-domain seismic data. It shows that almost 0–300 Hz of well log data can be preserved to generate the initial model during depth-domain seismic waveform indicator inversion. This can be used to improve not only the stability of the low-frequency components of the inversion result, but also the resulting certainty by constraining the range of the high frequency. Hence, the prestack depth-migrated seismic data can better identify thin layers than the prestack time-migrated data through seismic waveform indicator inversion and should be used for depth-domain inversion.
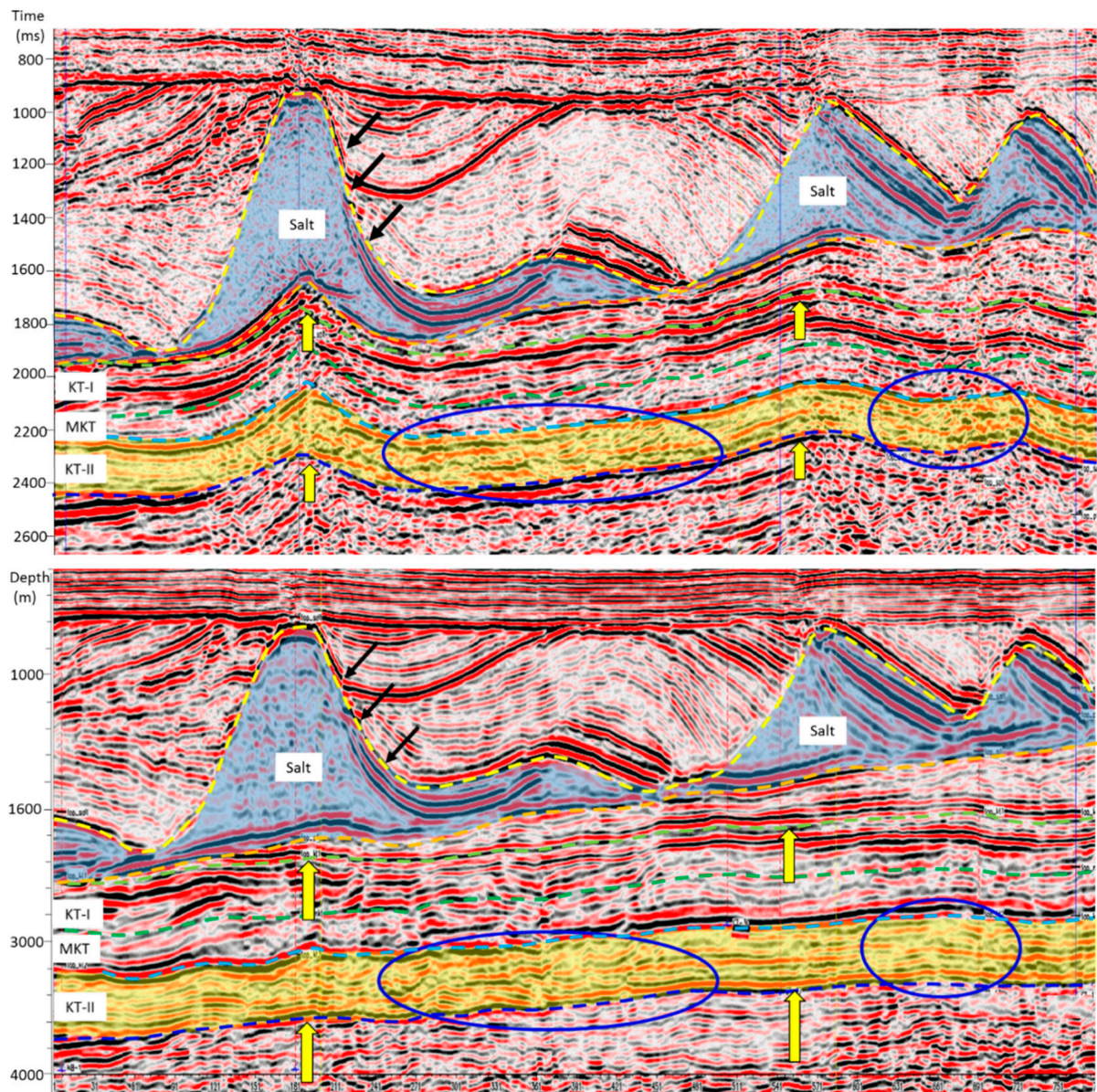
Figure 7. Comparison of prestack time-migrated seismic data (**upper**) and the reverse-time depth migrated seismic data (**lower**).

Table 1. Correlation coefficient of seismic waveforms and its corresponding frequency band-width of log curves. The first line is the statistical result of Figure 2.

Correlation Coefficient of Seismic Waveforms (Time)	Frequency Bandwidth of Log Curves in Time Domain (Hz)	Correlation Coefficient of Seismic Waveforms (Depth)	Frequency Bandwidth of Log Curves in Depth Domain (Hz)
0.81	0–200	0.79	0–300
0.73	0–200	0.75	0–300
0.68	0–100	0.64	0–200
0.84	0–200	0.82	0–300
0.77	0–200	0.77	0–200

3.3. Depth Domain Seismic Inversion

Sealed by MKT mudstone, Γ at the upper part of KT-II is the target reservoirs in the study area. Statistics show that single reservoir thickness of Γ_{1-2} is mostly approximately 1–4 m, as shown in Figure 8. The thin-layered carbonate reservoir is far below seismic resolution. It appears as a parallel/sub-parallel, continuous reflection without distinct architecture on the seismic section.
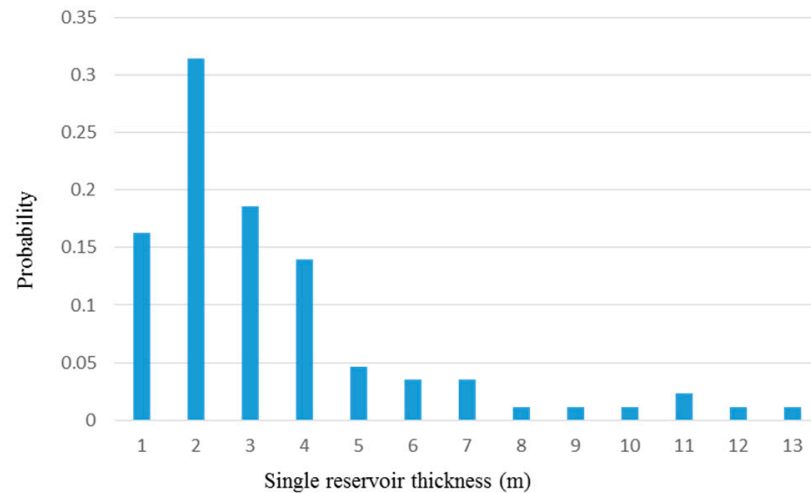

Figure 8. Statistic of single reservoir thickness of Γ_{1-2}, KT-II.

Based on the above analysis, to identify the presalt thin-layer carbonate reservoir, seismic waveform indicator inversion using prestack depth-migrated seismic data was selected. The seismic waveform indicator inversion using prestack time-migrated seismic data was also carried out to verify the estimation. Figure 9 shows the time-domain inversion result and depth-domain inversion result of Γ_{1-2} at the upper part of KT-II. Warm colors represent the reservoir, while cold colors stand for tight limestone. The seismic data is superimposed on the inversion result, showing the variation of seismic waveforms. Wells are attached to the inversion result, with interpreted reservoirs (red blocks). The time-domain inversion result shows a pull-up effect (yellow arrow) and has poor performance in recognizing thin reservoirs. The obvious anticlines in the time-domain profile do not exist in the depth-domain profile. It may cause problems if we use a time-domain profile to detect the potential hydrocarbon traps. Meanwhile, depth-domain inversion can provide a more accurate inversion result of the carbonate reservoir, which is consistent with the lithology distribution interpreted from well logging data.

The reservoir thickness map of Γ_{1-2} demonstrates patchy-shaped reservoir distribution, which is in accordance with the structure of beach deposition (Figure 10). Moreover, the eastern part of Central Block was previously thought to be an undeveloped area for carbonate reservoirs and, therefore, has never had a well drilled. Without much information, the seismic waveform indicator inversion result shows good reservoir development in the eastern part. Guided by the result, Well B was drilled, and its logging interpretation shows promising reservoir development at Γ_{1-2} of KT-II, which matches the inversion result very well (Figures 9 and 10).
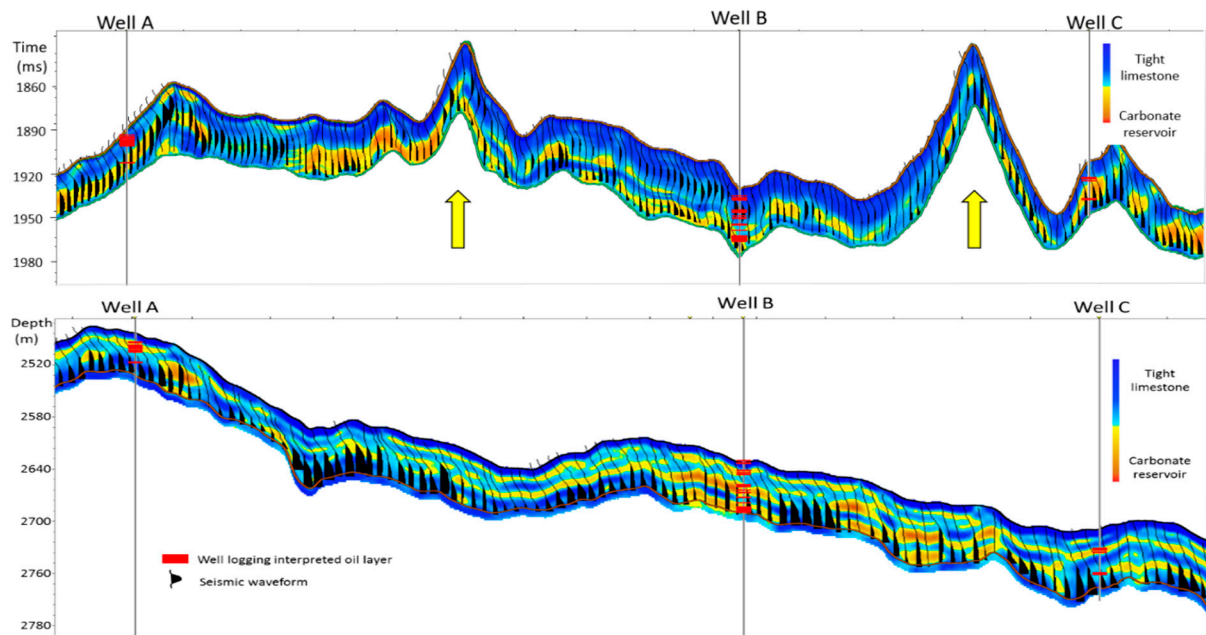
Figure 9. Time-domain inversion result (**upper**) and depth-domain inversion result (**lower**) of Γ_{1-2}, KT-II. See Figure 10 for the location of the profile.
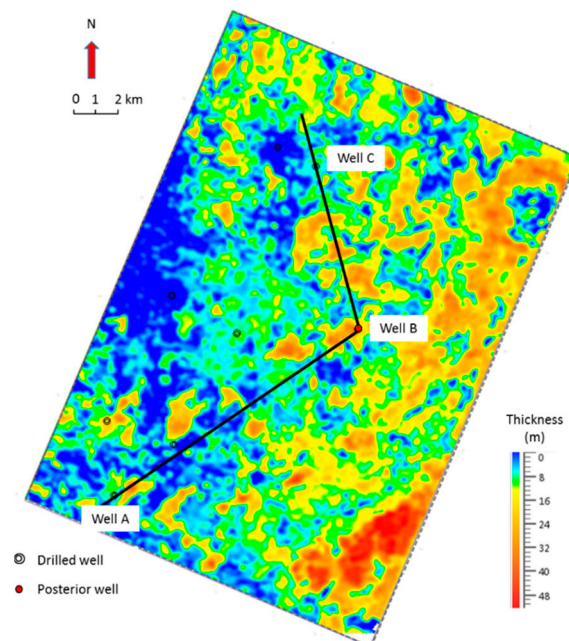

Figure 10. Reservoir thickness map of Γ_{1-2}, KT-II, showing that the carbonate reservoir is much developed in the eastern region of the study area.

4. Discussion

In this paper, we establish a method to quantitatively evaluate depth-domain and time-domain seismic data before seismic inversion and adopt the seismic waveform indicator inversion method for depth-domain seismic data inversion. Firstly, we built a geological model. From its corresponding prestack time migrated seismic reflection and depth migrated seismic reflection results, we can find out that seismic waveforms both in the time domain and in the depth domain are highly related to the lithology/reservoir properties. Thus, we can adopt the seismic waveform indicator inversion method to invert depth-migrated seismic data directly without depth-domain seismic wavelet extraction. Secondly, we proposed a quantitative evaluation method for time-domain and depth-domain seismic

data before inversion. Well log data have more high-frequency information than seismic data. By filtering log curves within the same sedimentary environment step by step, we can extract their common features. The final frequency band range of the common features determines the inversion effect. Therefore, it can help geophysicists decide whether it is worthwhile to conduct depth-domain seismic inversion. Finally, we applied the method to presalt thin carbonate reservoir prediction. Generally, the method we proposed in this paper has been proven to be both time and economically efficient and can be applied in other areas of seismic inversion studies.

Except for depth-domain seismic wavelet extraction, deterministic inversion methods based on the convolution model could only produce impedance results. Geostatistical inversion methods based on statistical analysis can directly estimate lithology and reservoir properties without depth-domain wavelet extraction, but the statistics of a variogram cannot accurately reflect the change in sedimentary facies in reservoir space. Moreover, depth-domain seismic data are rarely evaluated aiming at reservoir prediction before inversion. Since prestack depth migration is first and foremost aimed at improving structural imaging, in order to reduce calculation costs, information related to reservoir prediction may get lost due to different processing parameters. Therefore, it is very important to evaluate the depth-domain seismic data before inversion. The evaluation method mentioned in this paper is based on the relationship between seismic waveforms and well log data; it is also valuable for other inversion methods.

In a word, the reliability and accuracy of seismic inversion results highly depend on the quality of the seismic imaging, whether it is time-domain or depth-domain. Future studies should focus on the improvement of prestack depth-migrated data for seismic inversion. The mentioned seismic waveform analysis method can also be used in the seismic data processing procedure to determine reasonable processing parameters and strike a balance between calculation cost and data quality.

5. Conclusions

In this paper, we provide a depth-domain inversion method aiming at a more accurate structure and stable prediction result with a higher resolution and greater certainty. We suggest that the imaging quality of prestack depth migrated data must be evaluated before conducting depth-domain seismic inversion. Besides imaging quality evaluation for structure interpretation, a quantitative evaluation method of the data for reservoir prediction is also demonstrated. After data evaluation, we apply seismic waveform indicator inversion in the depth domain to predict the presalt thin carbonate reservoir in the Central Block at the eastern margin of the Pre-Caspian Basin. The depth-domain inversion produces not only a relatively true structure without pull-up effects, but also a higher resolution inversion result validated by wells. We believe that this method could be applied to other geologically complex environments where depth-migrated seismic data have better imaging quality.

Conflicts of Interest: The authors declare no conflict of interest.

References

1. Chahooki, M.Z.; Javaherian, A.; Saberi, M.R. Realization ranking of seismic geostatistical inversion based on a Bayesian lithofacies classification—A case study from an offshore field. *J. Appl. Geophys.* **2019**, *170*, 103814. [CrossRef]
2. Chopra, S. Inversion in Depth? *World Oil* **2016**, *17*. Available online: https://worldoil.com (accessed on 14 March 2023).
3. Macedo, I.D.; Silva, C.; Figueiredo, J.D.; Omoboya, B. Comparison between deterministic and statistical wavelet estimation methods through predictive deconvolution: Seismic to well tie example from the North Sea. *J. Appl. Geophys.* **2017**, *136*, 298–314. [CrossRef]
4. He, L.; Zhao, L.; Liu, R.; Li, J.; Wang, S.; Zhao, W.; Ma, J. Complex relationship between porosity and permeability of carbonate reservoirs and its controlling factors: A case of platform facies in Pre-Caspian Basin. *Pet. Explor. Dev.* **2014**, *41*, 206–214. [CrossRef]
5. Al-chalabi, M. Time-depth relationship for multi-layer depth conversion. *Geophys. Prospect.* **1997**, *45*, 471–486. [CrossRef]
6. White, R.E.; O'Brien, P.N.S. Estimation of the primary seismic pulse. *Geophys. Prospect.* **1974**, *22*, 627–651. [CrossRef]
7. Hu, Z.P.; Lin, B.X.; Xue, S.G. Depth domain wavelet analysis and convolution studies. *Oil Geophys. Prospect.* **2009**, *44*, 29–33.
8. Fletcher, R.P.; Archer, S.; Nichols, D.; Mao, W. Inversion after depth imaging. In Proceedings of the 82nd SEG Annual International Meeting, Expanded Abstracts, Las Vegas, NV, USA, 4–9 November 2012.
9. Chen, G.; Yang, W.; Liu, Y.; Wang, H.; Huang, X. Salt Structure Elastic Full Waveform Inversion Based on the Multi-scale Signed Envelope. *IEEE Trans. Geosci. Remote Sens.* **2022**, *60*, 1–12. [CrossRef]
10. Chen, G.; Yang, W.; Liu, Y.; Luo, J.; Jing, H. Envelope-based sparse constrained deconvolution for velocity model building. *IEEE Trans. Geosci. Remote Sens.* **2022**, *60*, 1–13. [CrossRef]
11. Singh, Y. Deterministic inversion of seismic data in the depth domain. *Lead. Edge* **2012**, *31*, 538–545. [CrossRef]
12. Fletcher, R.P.; Nichols, D.; Bloor, R.; Coates, R.T. Least-squares migration-Data domain versus image domain using point spread functions. *Lead. Edge* **2016**, *35*, 157–162. [CrossRef]
13. Zhang, J.L.; Xu, M.R.; Ye, Y.M. Seismogram synthetizing in the depth-domain with point spread function. *Oil Geophys. Prospect.* **2019**, *54*, 875–881.
14. Zhang, R.; Zhang, K.; Alekhue, J.E. Depth-domain seismic reflectivity inversion with compressed sensing technique. *Interpretation* **2017**, *5*, T1–T9. [CrossRef]
15. Zhang, R.; Deng, Z. A depth variant seismic wavelets extraction method for inversion of post-stack depth domain seismic data. *Geophysics* **2017**, *83*, R569–R579. [CrossRef]
16. Sun, Y.C. Geostatistical inversion based on Bayesian-MCMC algorithm and its applications in reservoir simulation. *J. Prog. Geophys.* **2018**, *33*, 724–729. [CrossRef]
17. Wang, K.Y.; Xiao, Z.J.; Jiang, Y.; Pang, S.Y.; Gao, Y.H. Seismic inversion method of stochastic stimulation in depth domain and its application. *Prog. Geophys.* **2017**, *32*, 1665–1672. (In Chinese) [CrossRef]
18. Chen, X.H. Depth domain geostatistical inversion of Fuyu Group in Chaoyanggou Oilfield. *Fault-Block Oil Gas Field* **2018**, *25*, 446–449.
19. Sun, S.M.; Peng, S.M. Inversion of geostatistics based on simulated annealing algorithm. *Oil Geophys. Prospect.* **2007**, *42*, 38–43.
20. Gu, W.; Xu, M.; Wang, D.H.; Zheng, H.; Zhang, X.; Zhang, D.J.; Luo, J. Application of seismic motion inverison technology in thin reservoir prediction: A case study of the thin sandstone gas reservoir in the B area of Junggar Basin. *Nat. Gas Geosci.* **2016**, *27*, 2064–2069.
21. Luo, H.M.; Wang, C.J.; Liu, S.H. Well-to-seismic calibration in the depth domain using dynamic depth warping. *Oil Geophys. Prospect.* **2018**, *53*, 997–1005.
22. Xu, K. *Hydrocarbon Accumulation Characteristics and Exploration Practices of Central Block in the Eastern Margin of the Pre-Caspian Basin*; Petroleum Industry Press: Beijing, China, 2011; Volume 6, pp. 30–33.
23. He, X.H. Discussion on seismic data of depth domain. *Geophys. Prospect. Pet.* **2004**, *43*, 353–358.
24. Kulumbetova, G.Y.; Nursultanova, S.G.; Mailybayev, R.M. Lithological types and reservoir properties of KT-II reservoir on the eastern edge of Pre-Caspian Basin. *Int. J. Eng. Res. Technol.* **2019**, *12*, 1335–1340.
25. Wang, Z.; Wang, Y.K.; Luo, M.; Ling, K.H.; Lin, Y.P. Carbonate depositional facies analysis and reservoir prediction for Central Block in Pre-Caspian Basin. *Adv. Mater. Res.* **2013**, *73*, 305–310.
26. Liu, W.Q.; Wang, X.W.; Liu, H.; Wang, Y.C.; Wang, X.; Zeng, H.H.; Shao, X.C. Application of velocity modeling and reverse time migration to subsalt structure. *Chinese J. Geophy.* **2013**, *56*, 616–625.